



# An injectable MB/BG@LG sustained release lipid gel with antibacterial and osteogenic properties for efficient treatment of chronic periodontitis in rats



Yeke Chen<sup>a,b,c,e,1</sup>, Fang Dai<sup>a,b,c,1</sup>, Tian Deng<sup>a,b,c</sup>, Lijie Wang<sup>a,b,c,e</sup>, Yuting Yang<sup>a,b,c,e</sup>,  
Chenjiang He<sup>a,b,c,e</sup>, Qiangdong Liu<sup>a,b,c,e</sup>, Jianxin Wu<sup>a,b,c</sup>, Fanrong Ai<sup>d,\*\*</sup>, Li Song<sup>a,b,c,\*</sup>

<sup>a</sup> Center of Stomatology, The Second Affiliated Hospital of Nanchang University, Nanchang, Jiangxi, 33006, China

<sup>b</sup> The Institute of Periodontal Disease, Nanchang University, Nanchang, Jiangxi, 33006, China

<sup>c</sup> JXHC Key Laboratory of Periodontology (The Second Affiliated Hospital of Nanchang University), Nanchang, Jiangxi, 33006, China

<sup>d</sup> School of Advanced Manufacturing, Nanchang University, Nanchang, Jiangxi, 33006, China

<sup>e</sup> The Second Clinical Medical School, Nanchang University, Nanchang, Jiangxi, 33006, China

## ARTICLE INFO

### Keywords:

Periodontitis  
Antimicrobial photodynamic therapy  
Periodontal regeneration  
Antiinflammation  
Sustained release

## ABSTRACT

Periodontitis is a chronic inflammatory disease characterized by the colonization of pathogenic microorganisms and the loss of periodontal supporting tissue. However, the existing local drug delivery system for periodontitis has some problems including subpar antibacterial impact, easy loss, and unsatisfactory periodontal regeneration. In this study, a multi-functional and sustained release drug delivery system (MB/BG@LG) was developed by encapsulating methylene blue (MB) and bioactive glass (BG) into the lipid gel (LG) precursor by MacroSOL technology. The properties of MB/BG@LG were characterized using a scanning electron microscope, a dynamic shear rotation rheometer, and a release curve. The results showed that MB/BG@LG could not only sustained release for 16 days, but also quickly fill the irregular bone defect caused by periodontitis through in situ hydration. Under 660 nm light irradiation, methylene blue-produced reactive oxygen species (ROS) can reduce local inflammatory response by inhibiting bacterial growth. In addition, *in vitro* and *in vivo* experiments have shown that MB/BG@LG can effectively promote periodontal tissue regeneration by reducing inflammatory response, promoting cell proliferation and osteogenic differentiation. In summary, MB/BG@LG exhibited excellent adhesion properties, self-assembly properties, and superior drug release control capabilities, which improved the clinical feasibility of its application in complex oral environments.

## 1. Introduction

Periodontitis is a chronic inflammatory disease caused by the interaction between host inflammatory response and oral pathogenic microorganisms [1], which ultimately leads to alveolar bone loss, periodontal pocket formation and irreparable damage to periodontal supporting tissue [2–4]. The current clinical therapy strategy for periodontitis involves the removal of subgingival plaque attachment through mechanical debridement (including scaling and root planning) and antimicrobial agents [5,6]. Mechanical debridement is time-consuming, expensive, and has limited therapeutic effects in sites that are difficult to reach instrumentally, such as root furcation, root concavities, and deep periodontal pockets. Additionally, systemic antimicrobial therapy not only has

insufficient effective concentration in the lesion area, but it also increases the risk of microbial resistance [7,8]. At present, a variety of tissue engineering materials used in the treatment of periodontitis have attracted strong attention from researchers, including scaffolds [9,10], hydrogels [11,12], and nanoparticle drug delivery systems [13,14]. As shown in Table S1, although these materials have achieved certain effects in the treatment of periodontitis, there are still some limitations. These deficiencies include difficulty in fitting irregular periodontal defects, insufficient adhesion strength to against oral saliva scour, drug burst release, short treatment time and single function. Therefore, it is an urgent need to develop a multi-functional long-release strategy for periodontitis treatment.

The objective of periodontal treatment is to inhibit periodontal

\* Corresponding author. Center of Stomatology, The Second Affiliated Hospital of Nanchang University, Nanchang, Jiangxi, 33006, China.

\*\* Corresponding author.

E-mail addresses: [afr3755875@126.com](mailto:afr3755875@126.com) (F. Ai), [ndefy91009@ncu.edu.cn](mailto:ndefy91009@ncu.edu.cn) (L. Song).

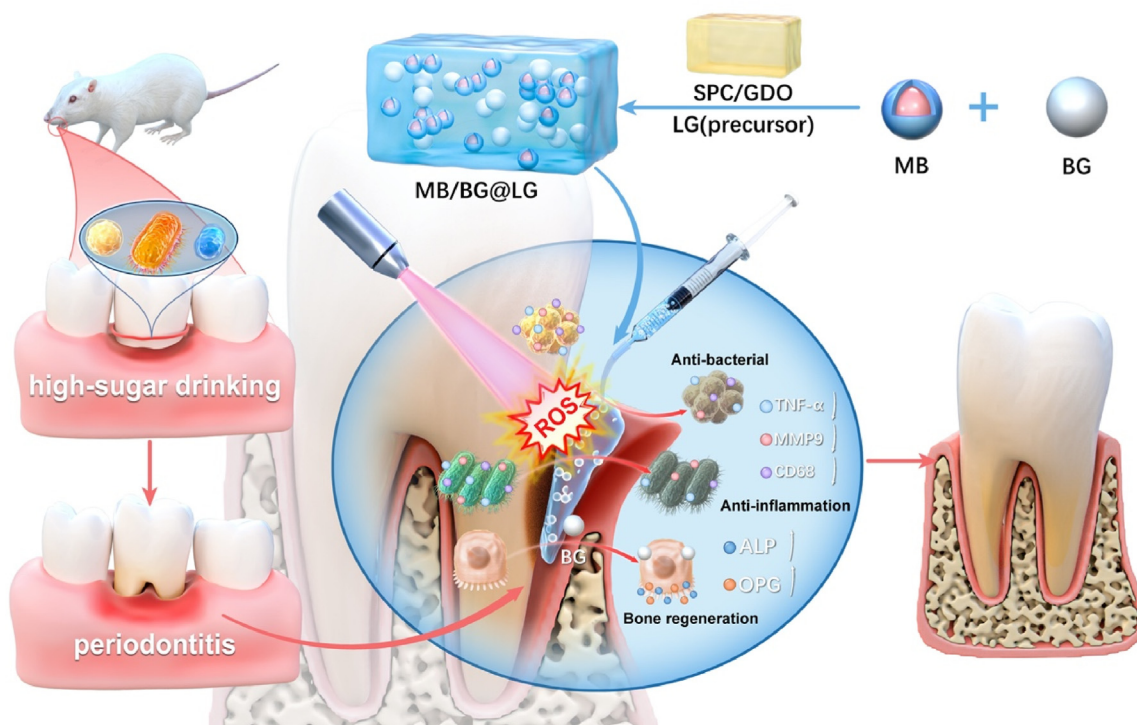
<sup>1</sup> These authors contribute equally to this work.

pathogens and accelerate periodontal bone regeneration [12,15,16]. In terms of antibacterial, compared with mechanical therapy and conventional chemotherapy, Antimicrobial photodynamic therapy (APDT) has unique advantages such as high spatiotemporal selectivity, broad spectrum, rapid release of reactive oxygen species (ROS) by external light to inhibit plaque with easy operation, and cooperativity with other treatments [17,18]. APDT is currently considered an attractive photochemical therapeutic tool against a variety of bacterial pathogens in the post-antibiotic era [19]. Methylene blue (MB) generates ROS by transferring energy to oxygen and other molecules during the fading from the active state to the ground state under specific wavelength irradiation [20]. ROS exert their biocidal activity by countering oxidative damage to biomolecular sites in the pathological target, such as phospholipids, proteins, DNA [21]. Meanwhile, methylene blue is the most widely used phenothiazine photosensitizer because of its excellent water solubility, low cost, and efficient generation of ROS under anaerobic conditions [22]. However, due to the complex environmental characteristics of the oral cavity (such as continuous saliva secretion, chewing, and tongue movement), the existing methylene blue delivery system is difficult to maintain at the lesion site in order to achieve a long-term therapeutic effect, which may lead to an unsatisfactory antibacterial effect and insignificant periodontal regeneration [23,24]. In the aspect of bone regeneration, bioactive glasses have attracted much attention as synthetic bone regenerative materials due to their capacity to transform hydroxyapatite, the natural mineral component of bone, to bind tightly to bone and stimulate the healing of bone defects by releasing ions [25]. Moreover, bioactive glass (BG) can support the proliferation and differentiation of osteoblasts and mesenchymal stem cells in vitro and in vivo [26]. Therefore, we are currently considering how to combine MB and BG into a complete system that can not only satisfy the effects of antibacterial, anti-inflammatory and bone regeneration, but also achieve the sustained release of MB for the treatment of periodontitis.

As continuous drug delivery carriers, lipid-based lyotropic depot matrices offer vast application possibilities in tissue engineering due to

their thermodynamic stability, biocompatibility, and favorable environment for tissue and cell growth [27,28]. In comparison to well researched lipids such as glycerol monooleate and phytotriol, the lipid gel (LG) produced of soybean lecithin choline (SPC) and glycerol dioleate (GDO) have excellent functional properties such as bioadhesion, excellent drug loading ability, enhanced self-assembly flexibility [28–31]. It can effectively be used for stable delivery and release of hydrophilic, lipophilic, and amphiphilic drugs [29,32]. The burst release of drugs (such as highly hydrophilic methylene blue) is minimized due to the excellent encapsulation properties of lipids [27,33,34]. Therefore, this lipid gel system can be employed as a platform for continuous medicine administration in periodontal therapy.

In this study, we innovatively synthesized a lipid gel by mixing BG and MB into a lipid mixture (LG precursor) of soybean phosphatidylcholine (SPC) and dioleate glycerol (GDO) in an all-in-one manner. It perfectly solves the problem that MB preparation is not easy to retain and burst release in the lesion site. Owing to the excellent encapsulation performance of the lipid, the effective release of MB in the system reached over 14 days in vitro. After injecting MB/BG@LG into the periodontal pocket, the LG precursor can undergo in situ hydration and can be immediately gelled in a moist oral environment to fill irregular bone defects caused by periodontitis and qualify for addressing the specific requirements of patients in clinical practice. Simultaneously, MB under manually controlled visible irradiation can generate ROS to inhibit periodontitis pathogens, achieve antibacterial effects, and alleviate inflammation. Osteogenic-related protein production and periodontal bone repair can be stimulated by BG and the ions released. We evaluated the anti-inflammatory, antibacterial, and osteogenic effects of BG/MG@LG in periodontitis rats. The results showed that alveolar bone regeneration was significant and inflammatory factors were suppressed after BG/MG@LG injection. Therefore, we believe that BG/MG@LG is a potent alternative therapy for the treatment of periodontitis that can meet the specific needs of different patients in clinical practice. (see Scheme 1)



**Scheme 1.** Scheme of the synthesis process, antibacterial effects, anti-inflammatory effects, and promotion of periodontal regeneration of injectable MB/BG@LG.

## 2. Methods

### 2.1. Preparation of the MB/BG@LG

According to previously described preparation methods, the drug-loaded LG precursor was manufactured via the “Macrosol” technique [28]. The first step was to prepare the lyophilized system. 100 mg SPC (Shanghai Yuanye, product number S27923) and 60 mg BG were added to 0.5 mL of 1 mM MB (Sigma-Aldrich, product number M9140) aqueous solution. After thorough mixing on a roller mixer, the mixture was lyophilized (TDZ5-WS, China) to obtain the lyophilized system. Next, SPC and GDO (Shanghai Yuanye, product number B28313) were evenly mixed at a ratio of 35/65 and 10% absolute ethanol was added to obtain the oil phase precursor preparation of LG. Subsequently, the lyophilized system mentioned above was mixed with 1.0 g of the precursor at ambient temperature on a rolling mixer until the non-aqueous mixture became a homogeneous lipid solution formulation of MB/BG@LG.

### 2.2. Characterization

Scanning electron microscopy (SEM; Zeiss, Germany) was used to evaluate the appearance of the lyophilized system of MB/BG@LG. The elemental mapping of the materials was performed by combining scanning electron microscopy with energy dispersive spectroscopy (EDS; Inca Energy, England). Dynamic light scattering (DLS, Malvern Instruments, UK) was used to measure the bioglass diameter. Flight Test Instrumentation Requirements (FTIR; Thermo Scientific Nicolet iS20, USA) were performed to analyze the composition of MB/BG@LG. The morphology before and after release was observed by cryo-electron microscopy. (Cryo-SEM; Hitachi Regulus 8220; Japan).

### 2.3. The sol-gel phase transition

In a glass container with a lid, a specific quantity of the LG precursor was introduced together with a small amount of water. The test tube inversion approach was used to describe the transition of the sol-gel characteristics.

### 2.4. In vitro adhesion of MB/BG@LG

The shear adhesion strength of MB/BG@LG was measured on glass by the universal tensile tester. The overlapping area between MB/BG@LG and glass slide was 25 mm × 20 mm. Shear adhesive strength was tested with a universal tensile testing machine at a strain rate of 20 mm min<sup>-1</sup>. Each experiment was repeated three times.

The adhesion of MB/BG@LG to alveolar bone of rats was tested by oral saliva simulation experiment. First, MB/BG@LG was injected into the alveolar bone followed by a small amount of water to quickly self-assemble into a gelatinous system. The gelled MB/BG@LG was flushed with running water to test its adhesion strength.

### 2.5. Rheological analysis and viscosity analysis

Rheological and viscosity analyses were conducted using a dynamic shear rotary rheometer. (ThermoFisher, America). Two grams of prepared MB/BG@LG were placed at the center of the rheometer plate and equilibrated at room temperature for 5 min before beginning any experiment. Peristaltic scanning was used to measure the shear viscosity ( $\eta$ ) at shear rates ranging from 1 to 120 s<sup>-1</sup>. Rheological tests were conducted within the range of 0–10 min, and the storage modulus ( $G'$ ) and loss modulus ( $G''$ ) of the rheological parameters were calculated to study the sol-gel transition behavior during the formation of liposomes with angular frequency ( $\omega$ ) and strain ( $\gamma$ ) fixed at 2 rad/s and 5%, respectively.

### 2.6. In vitro drug release

In each light-protected tube, 1 mL MB/BG@LG was added to 5 mL PBS and incubated on a thermostatic shaker (37 °C, 100rpm). At pre-determined intervals, a fresh 1.5 mL of PBS solution was added to the vial, while 1.5 mL of the medium was removed and stored at -4 °C for further analysis. The cumulative release of methylene blue was determined using an ultraviolet spectrophotometer (Nikon, Japan).

### 2.7 light-triggered generation of reactive oxygen species (ROS)

The light-triggered singlet oxygen of MB/BG@LG was quantified using 1,3-diphenylisobenzofuran (DPBF) (MedChemexpress, USA) as a probe. Briefly, 0.3 mL of saturated dimethylformamide (DMF) containing DPBF (200 µg/mL) was added to 2.7 mL of MB/BG@LG impregnated solution or MB solution (equivalent to MB/BG@LG). The mixture was kept in the dark under constant stirring and irradiated with a 660 nm laser at an output power of 100 mW/cm<sup>2</sup>. The absorbance of the solution was measured using an ultraviolet spectrophotometer.

### 2.8. Photodynamic antibacterial in vitro

*Staphylococcus aureus* (ATCC 6538) and *Escherichia coli* (ATCC 25922) and *Porphyromonas gingivalis* (ATCC BAA-308 W83) were used to evaluate the antibacterial activity of MB/BG@LG. The 0.1 mL bacterial solution (1.0 × 10<sup>8</sup> CFU/mL) and 0.1 mL MB/BG@LG impregnated solution diluent in different multiples were placed in a 96-well plate and incubated in the dark for half an hour. Then, the plates of the light group were exposed to a 660 nm laser for 3 min. The plate counting method was used to assess the antibacterial capabilities. To stain bacteria, N01/propidium iodide was used as directed by the LIVE/DEAD bacterial kit (Solarbio, China). Images of dead bacteria colored red and live bacteria-stained green was observed using inverted fluorescence microscopy. At the same time, the morphological changes of the bacteria in each group were observed under a scanning electron microscope.

### 2.9. Biocompatibility in vitro

Hemolysis Assay: Following the accepted experimental protocol, blood was drawn from Sprague-Dawley (SD) rats. The fresh rat blood was separated from the plasma by centrifugation at 3000 rpm for 10 min at 4 °C. The isolated RBCs were washed with PBS until the supernatant was limpid, and then diluted to 5% (v/v) with PBS. Deionized water, saline solution, and a progressive percentage of MB/BG@LG impregnated solution were added to the diluted red blood cells. The supernatants from each group were collected, and the absorbance at 562 nm was determined after incubation at 37 °C for 1 h. The following formula was used to determine the hemolysis rate:

$$\text{Hemolysis (\%)} = \frac{A_s - A_n}{A_p - A_n} \times 100\%$$

where  $A_s$ ,  $A_p$ , and  $A_n$  represent the absorbance values of the MB/BG@LG extract (sample group), distilled water (positive control group), and saline (negative control group), respectively.

Cell viability: The proliferation and viability of L929 and MC3T3-E1 cells (iCell, China) were evaluated using the CCK-8 Assay Kit (Servicebio, China). For cell viability, L929 cells and MC3T3-E1 cells were consecutively placed on 96-well microdroplet plates at a density of 5 × 10<sup>3</sup> cells/well and then cocultured with sample impregnated solutions for 1, 3, and 5 days. The incubation was maintained at 37 °C for 2 h after the introduction of 100 µl of CCK-8 mixture. Finally, a microplate reader was used to measure the absorbance at 450 nm. The following formula was implemented to compute cell viability:

$$\text{Cell viability} = \text{OD}_{\text{sample}} / \text{OD}_{\text{control}}$$

For live/dead cell staining, L929 and MC3t3-E1 cells were seeded on 24-well microdroplet plates at a density of  $1.0 \times 10^4$  cells/well and incubated for 24 h under the above-mentioned conditions. The original culture medium was replaced with the impregnated solution of the sample and cultured for one or three days. After dark incubation with 300  $\mu$ l of calcein-AM/PI (Yeasen, China) staining solution for 30 min, red-stained dead cells and green-stained live cells were distinguished by inverted fluorescence microscopy. The light group in the experiment received 3 min of exposure to a 660 nm laser at a power density of 100 mW/cm<sup>2</sup>, and three duplicates of each experiment were carried out.

SEM image of MC3t3-E1 cells: MC3t3-E1 cells were inoculated on silicon wafers at a density of  $1.0 \times 10^4$  cells/well and incubated with the sample impregnated solution for 24 h. Next, the cells on the silicon wafer were dehydrated and fixed according to sample preparation requirements. SEM was used to examine the morphology and migration status of MC3t3-E1 cells.

### 2.10. Osteogenic differentiation of MC3t3-E1 in vitro

MC3t3-E1 cells at the logarithmic growth stage were inoculated in 24-well culture plates ( $1.0 \times 10^5$  cells per well) and co-cultured with osteogenic induction medium with or without the impregnated solution of MB/BG@LG and LG for 7 or 14 days. After co-culture, MC3t3-E1 cells were first fixed with 4% paraformaldehyde, gently washed three times with PBS and stained with the AKP/ALP kit (Beyotime, China). After incubation for 20 min at room temperature in the dark, the cell staining was observed under an optical microscope. The alp activity kit (Nanjing Jiancheng; China) was used for quantitative analysis.

### 2.11. In vivo biodegradation and biocompatibility

All animal protocols were approved in accordance with the Guidelines for the Care and Use of Laboratory Animals of Nanchang University in China and were approved by the Animal Ethics Committee of Nanchang University (NCULAE-202209280026). Eight-week-old female SD rats were obtained from Changsha Tianqin Biotechnology Co, Ltd. (Changsha Tianqin, China) for the in vivo experiments. First, SD rats were anesthetized and 200  $\mu$ l of sterile MB/BG@LG or LG precursor was injected subcutaneously into the backs of SD rats. On days 3, 7, 14, 28, and 56, the rats were euthanized, Hematoxylin and eosin (H&E) staining was used to analyze subcutaneous degradation and potential inflammatory reactions. In the experiment, the light group was exposed to a 660 nm laser at a power density of 100 mW/cm<sup>2</sup> for 3 min.

### 2.12. Establishment of the rats periodontitis model and treatment

The therapeutic effects of MB/BG@LG on periodontitis were observed in 8 weeks female SD rats and randomly separated into six groups (N = 3/group). Based on previous reports, chronic periodontitis was induced by silk ligation combined with high glucose feeding. Briefly, the rats were anesthetized for the experiment. Then the 4-0 non-absorbable sutures were positioned subgingival on either side of the maxillary second molars (M2) without damaging the nearby gingival tissues, and the rats were daily given a high-sugar (10% sucrose) diet. After ligation placement for 3 weeks, the ligatures were removed. Different treatments were locally administered every 3 days for 2 weeks with MB/BG @LG or LG around M2. The six groups were defined as healthy (healthy rat), periodontitis (ligation), control (untreated after ligature removal), LG (treated with LG after ligature removal), MB/BG @LG + Light (treated with MB/BG @LG + Light after ligature removal), and MB/BG @LG -Light (treated with MB/BG @LG - Light after ligature removal). At the end of the 4th week, all rats were euthanized with an overdose of the anesthetic. Gingival tissue was extracted from the buccal and lingual sides of M2. The concentration of tumor necrosis factor- $\alpha$  (TNF- $\alpha$ ) was determined using ELISA kits (MultiSciences, China). For further analyses, all three maxillary molars, alveolar bone, and attached

gingival tissues were collected and preserved in a 4% paraformaldehyde solution.

### 2.13. Micro computed tomography (micro-CT) analysis

A micro-CT system was used to analyze the ligated molar and the surrounding upper alveolar bone. Mimics software (version 21.0) was used to analyze the osteogenic ability of MB/BG@LG by measuring bone volume (BV), tissue volume (TV), BV/TV, and the distance between the alveolar bone crest the cement-enamel junction (CEJ-ABC).

### 2.14. Immunohistochemical and histological evaluation

After micro-CT detection, the samples were subjected to routine operations, including decalcification, dehydration, embedding in paraffin, and sectioning. Hematoxylin-eosin (H&E) and osteoprotegerin (OPG) staining were used to observe histological changes and osteoblast activity in the periodontal tissue. CD68 fluorescence staining and MMP9 immunohistochemistry were used to quantitatively analyze the total macrophages and inflammation levels in gingival tissues. In addition, the toxicity of MB/BG@LG was assessed using histopathological images of the heart, liver, spleen, lungs, and kidneys.

### 2.15. Statistical analysis

All statistical analyses were performed using GraphPad Prism 8 using one-way analysis of variance (ANOVA). Numerical data are shown as mean  $\pm$  standard deviation (SD). T-test was used to analyze the differences between the two groups of data. “\*” =  $p < 0.05$ , “\*\*” =  $p < 0.01$ , “\*\*\*” =  $p < 0.001$ .

## Result and discussion

### 3.1. Synthesis and characterization of MB/BG@LG

MB@BG/LG was synthesized by encapsulating the hydrophilic photosensitizer methylene blue and bioactive glass in the liposome precursor of LG using Macrosol technology. The surface and cross-sectional morphology of the lyophilized system of MB/BG@LG were observed using SEM. The lyophilized system of MB/BG@LG surface developed a porous structure coated with bioactive glass, which was conducive to the continuous release of methylene blue and bioactive glass while providing a three-dimensional space for cell growth (Fig. 1a and b). Further investigation of the elemental distribution in MB/BG@LG was performed using energy spectrum analysis. The presence of silicon, calcium, and other elements in the system further indicated that the bioactive glass was successfully encapsulated by the liposomes (Fig. 1c). The particle size of the bioglass was determined by dynamic light scattering. The average particle size of 90% of the bioglass was 53.4  $\mu$ m (Fig. 1d). In the FTIR spectrum (Fig. 1e), the peaks at 2922cm<sup>-1</sup>, 1739cm<sup>-1</sup> and 1168cm<sup>-1</sup> corresponded to the valence oscillations of C-H, C=O and C-O respectively [35]. All these characteristic peaks are key evidence for the ester structure in the lipid gel and MB/BG@LG. The bands 1612 cm<sup>-1</sup> and 1393 cm<sup>-1</sup> were ring and stretch vibrations of C-N groups in the MB molecule [36]. Interestingly, similar peaks appeared in the corresponding positions of MB and MB/BG@LG, but not in LG alone, indicating that MB was successfully wrapped in MB/BG@LG. Meanwhile, Si-O-Si key peaks appeared in BG and MB/BG@LG at 563 cm<sup>-1</sup> [37], indicating that BG was also successfully wrapped. The above results proved that MB/BG@LG loaded with MB and BG was synthesized successfully. At the same time, the ability of MB/BG@LG to release methylene blue was determined by an in vitro drug release experiment. The results demonstrated that methylene blue was released in vitro throughout the period of 16 days, and the total amount released was 76.87% (Fig. 1f). The excellent encapsulation properties and porous structure of the lipid gel ensured long-term sustained release of methylene blue. We further attempted to

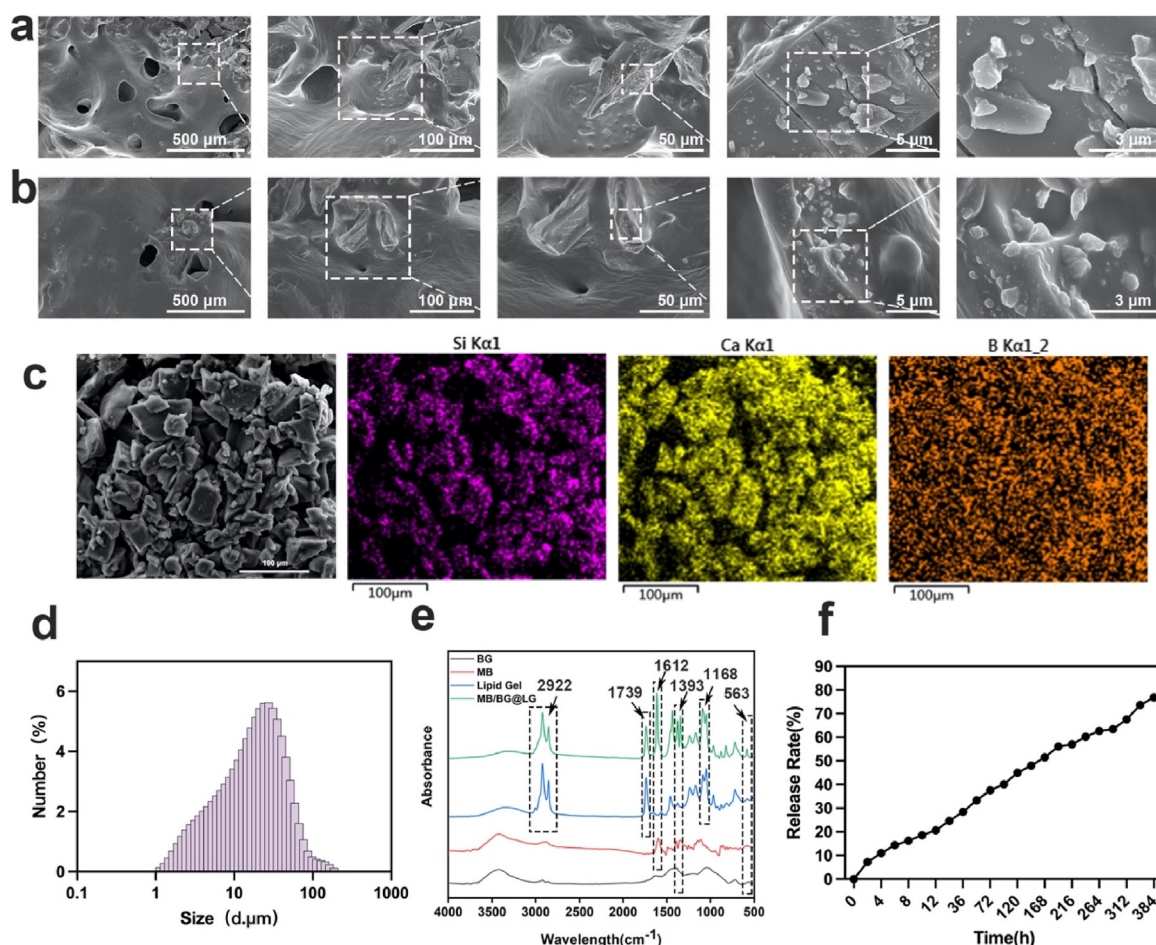


**Fig. 1.** The SEM images of the surface (a) and cross-sectional sides (b) of the lyophilized system of MB/BG@LG (The latter image is a partial magnification of the boxed region in the previous image); (c) The EDS analysis of MB/BG@LG. (d) The particle size distribution of bioglass. (e) The FTIR spectra of BG, MB, LG, MB/BG@LG. (f) The release rate of MB in MB/BG@LG at different times.

use cry-electron microscopy (Cryo-SEM; Hitachi Regulus 8220; Japan) to observe the changes of MB/BG@LG before and after 7 days of release. Before and after release, MB/BG@LG still maintained the original stable structure and a large amount of bioglass was still wrapped in it (Fig. S1). This system effectively avoids the transient burst release of MB and offers the potential of a long-term antibacterial effect of MB/BG@LG in the treatment of periodontitis.

To demonstrate the injectability and plasticity properties of MB/BG@LG, real images of the sol and gel phase transitions of MB/BG@LG are shown in Fig. 2a. When MB/BG@LG was injected into an aqueous solution with a 1 mL syringe, MB/BG@LG rapidly changed from a sol state to a gel state and formed stable lipid droplets in water (Fig. 2b and Movie 1). Next, we used a syringe dripping water to simulate the continuous production of saliva in the mouth. After MB/BG@LG was injected into the alveolar bone area of the mandible of rats, MB/BG@LG formed a gel immediately upon contact with water and remained static in the diseased area under continuous dripping (Fig. 2c and Movie 2). The shear adhesion strength of MB/BG@LG was tested using the slide method. According to S2 a-c, the shear strength of MB/BG@LG was  $0.05 \pm 0.018\text{KPa}$ . This indicated that the system had excellent adhesion properties and self-setting ability [31,38], which was suitable for application in moist oral environment. In addition, MB/BG@LG was injected into a predesigned irregular mold, and the gel was appropriately filled into the mold, indicating that the MB/BG@LG exhibited excellent plasticity (Fig. 2d). Based on the above experiments, it was determined that MB/BG@LG has good injectability and plasticity, as well as the ability to

gelatinize immediately in aqueous solution. This allows it to perfectly adapt to the different shapes of alveolar bone defects caused by periodontitis and form a gel in situ at corresponding sites using excessive gingival crevicular fluid and saliva exudate caused by inflammation. The rheological properties of MB/BG@LG were examined using a dynamic-shear rotational rheometer. Compared with the sol state, the gelatinized MB/BG@LG exhibited distinct non-hydrodynamic behavior, and its viscosity increased significantly after contact with the aqueous solution (Fig. 2e and f). MB/BG@LG was then mixed with a small amount of water to immediately measure the changes in  $G'$  and  $G''$  over time. As illustrated in Fig. 2g,  $G'$  was initially smaller than  $G''$ , indicating that MB/BG@LG was in the sol state. After a period of mixing,  $G'$  was greater than  $G''$ , indicating that MB/BG@LG successfully completed the sol-to-gel conversion. Then, we measured the change in  $G'$  and  $G''$  with frequency using gelatinized MB/BG@LG (Fig. 2h). As the frequency increased,  $G'$  was always larger than  $G''$ , indicating that MB/BG@LG was still in the gel state and had a certain degree of stability. The change in the shear frequency had no effect on its performance.

Supplementary data related to this article can be found online at <http://doi.org/10.1016/j.mtbio.2023.100699>

Supplementary data related to this article can be found online at <http://doi.org/10.1016/j.mtbio.2023.100699>

### 3.2. Measurement of singlet oxygen generation

DPBF was used as a probe to evaluate the ability of MB/BG@LG to

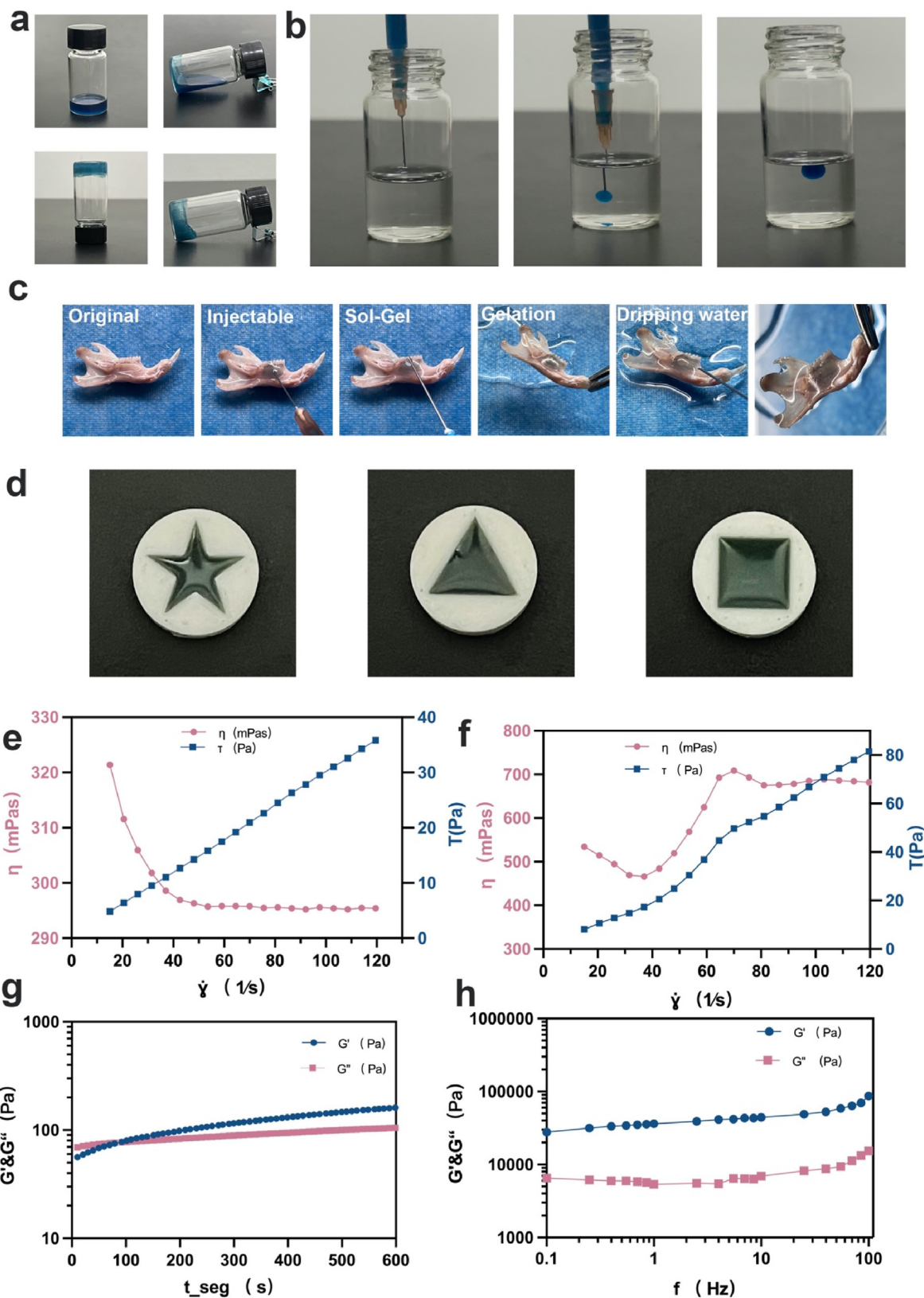


**Fig. 2.** (a) The photograph of MB/BG@LG before and after gelatinization. (b) The injectable property of MB/BG@LG (Movie 1). (c) Experiments simulating the effect of oral saliva flow on MB/BG@LG adhesion (Movie 2). (d)The plasticity property of MB/BG@LG. The viscosity varies and the shear stress changes with the shear rate of MB/BG@LG before gelatinization (e) and MB/BG@LG after gelatinization(f). (g) Time-responsive  $G'$  and  $G''$  modulus changes of MB/BG@LG in the process of sol-gel transition. (h) Frequency -responsive  $G'$  and  $G''$  modulus changes of MB/BG@LG after gelatinization.

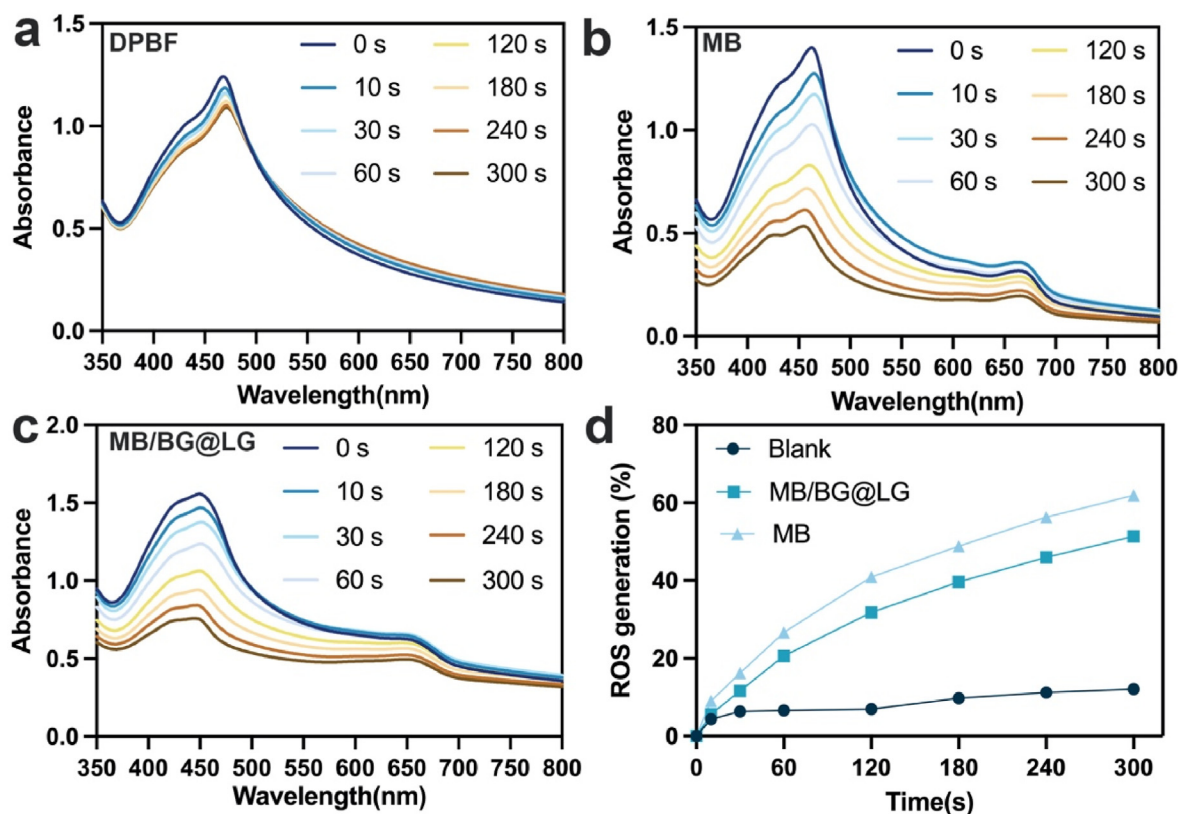


Fig. 3. The UV spectra of PBS(a), MB(b), MB/BG@LG(c) under 660 nm illumination at different times. The ROS generation rate(d) of Blank, MB/BG@LG, MB.

generate singlet oxygen under 660-nm light. The primary factor guaranteeing the validity of this experiment was the photostability of DPBF [39]. Fig. 3a shows that the variation of DPBF was negligible at different time intervals of exposure to 660 nm light irradiation. In contrast, both MB/BG@LG and comparable amounts of methylene blue solution after illumination showed significant consumption rates of DPBF, indicating a similar capacity to generate singlet oxygen (Fig. 3b and c). After exposure to light for 60 and 180 s, the singlet oxygen yields of MB/BG@LG reached 20.63% and 39.62%, respectively (Fig. 3d). This indicated that methylene blue can be released efficiently from the MB/BG@LG and that the material itself would not affect the photosensitivity of methylene blue, which has also been observed in other methylene blue loaded materials [40]. In addition, there was a special absorption peak of methylene blue at 662 nm in the UV-VIS spectrum [41]. In Fig. 3b and c, methylene blue was continuously consumed as the light time increased. Overall, these results revealed that the MB/BG@LG can serve as a photodynamic agent to treat periodontitis, in which bacterial infection was the main causative factor.

### 3.3. In vitro photodynamic antibacterial ability

Periodontitis has been widely recognized as a chronic inflammatory disease associated with bacterial infections. Long-term and persistent bacterial presence not only causes irreversible damage to periodontal supporting tissues, but it also has systemic health implications [42]. Based on previous results, MB has been extensively studied for its promising and effective photodynamic capabilities in photodynamic antimicrobial therapy [40]. Therefore, representative gram-positive (*Staphylococcus aureus*) and gram-negative (*Escherichia coli*) bacteria were used to test the in vitro antibacterial effects of MB/BG@LG. The antibacterial effects of MB/BG@LG impregnated solution with different concentration gradients under light were studied using the agar plate assay method. Fig. 4a and 4c show a physical representation of the bacterial plate counting method, with the number of colonies

significantly lower in the MB/BG@LG + Light group than in the PBS, PBS + Light, and MB/BG@LG -Light groups. A quantitative analysis of the number of colonies forming units (CFU) is shown in Fig. 4b,d. The CFU of *S. aureus* in the MB/BG@LG + Light, 1/2 MB/BG@LG + Light, 1/4 MB/BG@LG + Light groups and 1/8 MB/BG@LG + Light groups were  $0.48 \pm 0.06$ ,  $4.06 \pm 0.56$ ,  $6.45 \pm 1.10$ ,  $10.13 \pm 1.00 \times 10^7/\text{mL}$ , respectively, which were significantly less than those in the PBS group and PBS + Light ( $12.73 \pm 2.51$ ,  $13.29 \pm 1.91 \times 10^7/\text{mL}$ ), similar results were seen at *E. coli*. Compared with the PBS group. There was the discernible difference in the antibacterial effect between the MB/BG@LG + Light and MB/BG@LG -Light groups until dilution to 1/4 concentration, indicating that our material still has strong application potential in the presence of continuous saliva and gingival crevicular fluid dilution in the oral microenvironment. At the same time, the unilluminated group did not show a decrease in the number of colonies, indicating that MB/BG@LG could produce singlet oxygen only under the irradiation of excitation light at a fixed wavelength, which could impede the growth of bacteria [43]. A similar phenomenon was observed in the antibacterial test for *Escherichia coli*. These results indicate that singlet oxygen produced by photodynamic has a broad-spectrum antibacterial effect on gram-positive and gram-negative bacteria [44].

N01/PI staining was used to determine live/dead bacteria to further explore the antibacterial ability of MB/BG@LG under light. The N01 probe could penetrate the intact plasma membrane of living bacteria and react with DNA/RNA to produce the strongest green fluorescence signal. The probe for dead bacteria with membrane damage was PI, which is a red fluorescent nucleic acid stain representing damaged bacteria [45]. In the MB/BG@LG + Light group, both *Staphylococcus aureus* and *E. coli* had many PI positive expressions, indicating that MB/BG@LG exhibited strong antibacterial activity by destroying the integrity of the bacterial biofilm, leading to bacterial death caused by ROS generated during light exposure (Fig. 4e and f).

In addition, SEM was used to observe the integrity of bacterial cell

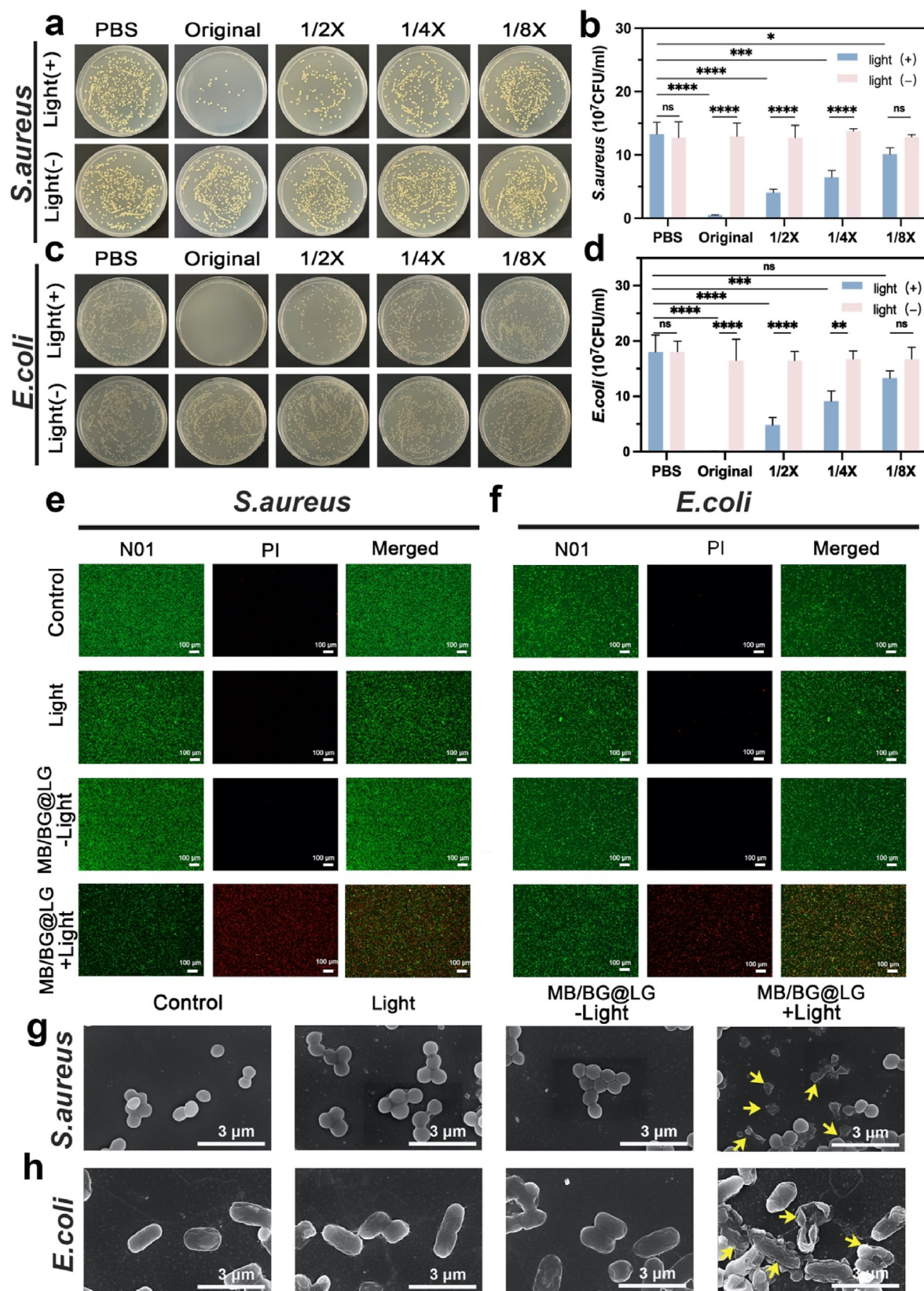
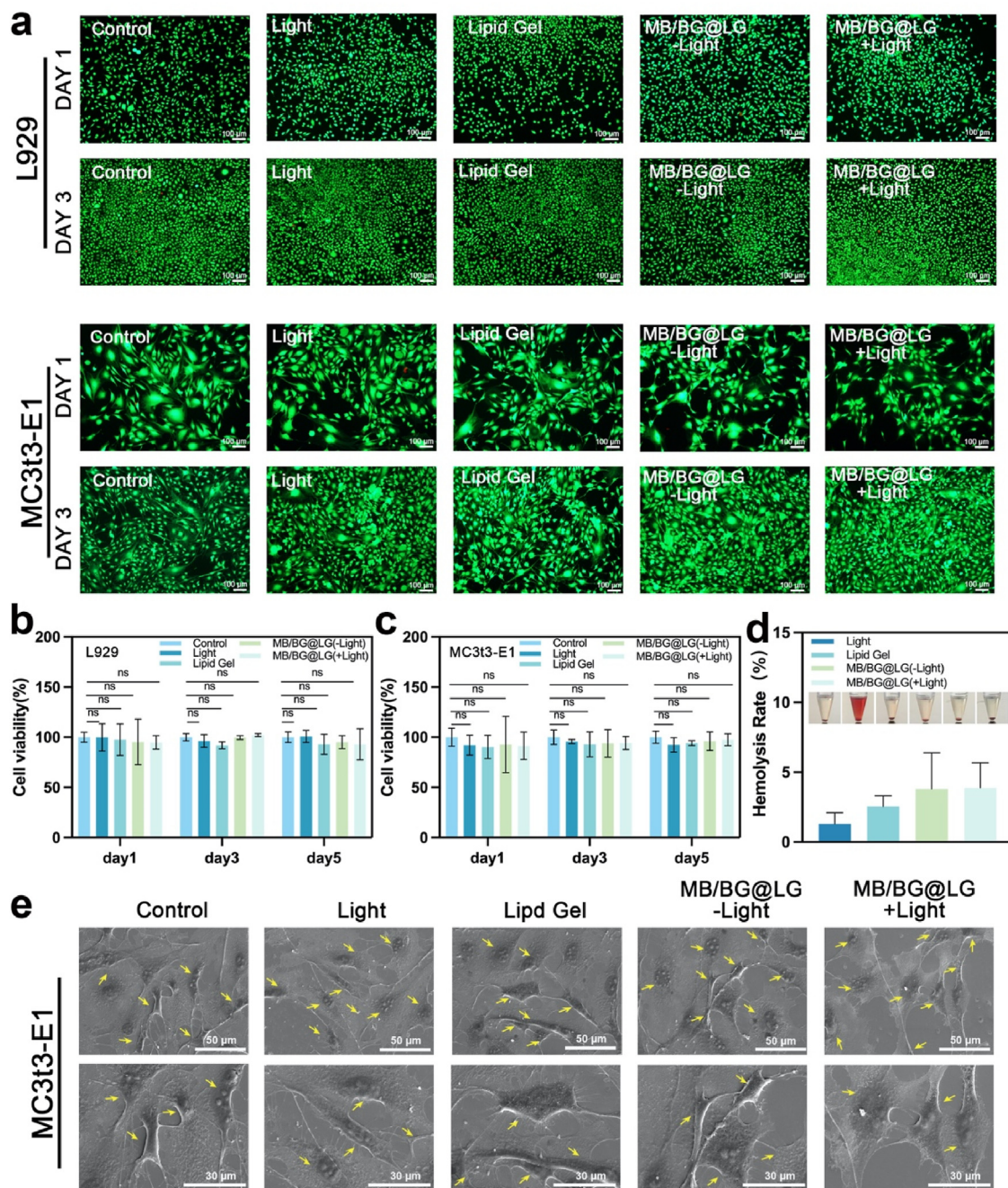


Fig. 4. Evaluation of the MB/BG@LG in vitro antibacterial properties. The images and quantitative analysis of *S. aureus* (a, b) or *E. coli* (c, d) bacterial colony treated with PBS and MB/BG@LG released fluid at different concentrations with and without 660 nm light. The SEM photograph of *S. aureus* (g) or *E. coli* (h) cultured with PBS and the impregnated solution of MB/BG@LG for 3 min with and without 660 nm light.



**Fig. 5.** (a) The Live/Dead staining images of L929 and MC3t3-E1 cultured with MB/BG@LG culture medium on days 1 and 3. The cell viability of L929(b) and MC3t3-E1(c) cultured with MB/BG@LG culture medium on days 1, 3, and 5. (d) The hemolysis rate of Light, LG, MB/BG@LG (-light), and MB/BG@LG (+light) groups. (e) The SEM photographs of MC3t3-E1 cultured with MB/BG@LG culture medium for 24 h.

walls. Compared with other groups, SEM images clearly showed that the cell walls of *Staphylococcus aureus* and *Escherichia coli*, the MB/BG@LG + Light group had varying degrees of shrinkage and rupture (Fig. 4g and h, respectively).

We further select *porphyromonas gingivalis*, a pathogen causing periodontitis [46], for antibacterial experiment. To observe the effects of MB/BG@LG more directly on bacterial cell walls, representative images of the bacteria after MB/BG@LG were taken using a scanning electron microscope (Fig. S3). Normal *porphyromonas gingivalis* showed typical

short rod-like shape, while *porphyromonas gingivalis* in MB/BG@LG (+Light) group showed contraction and even collapse, which indicated that our material also had killing effect on bacteria.

These results indicated that APDT-based MB/BG@LG had the expected antimicrobial activity and could adapt to a moist oral environment. It exhibited potent antibacterial activity when diluted in saliva and inflammatory exudates. MB/BG@LG could be a highly selective, broad-spectrum, rapid, and effective method for combating pathogenic microorganisms.

3.4. Biocompatibility and hemocompatibility of MB/BG@LG

Excellent biocompatibility is the key point to maintaining cell viability and proliferation and is also a prerequisite for materials to be applied in the biomedical field. First, we performed dead and live staining experiments. Calcine-AM labeled the living cells green, whereas PI penetrated the dead cells and caused them to produce spectacular red fluorescence. Fig. 5a demonstrates that most of the cells in each group were green and had the typical spindle-like shape of L929 cells. After the third day of co-culture, obvious proliferation and excellent cell viability were still observed. The CCK-8 assay was used to determine the cytotoxicity of the materials on L929 and MC3t3-E1 cells. After 1, 3, and 5

days of co-culture, the survival rates of cells in the control, light, MB/BG@LG + Light, and MB/BG@LG -Light groups were all greater than 90%, and cell proliferation was active (Fig. 5b and c), similar to the dead/live staining results. In addition, we performed an in vitro hemolysis assay to further verify the biocompatibility of MB/BG@LG. The findings demonstrated that less than 5% [47] of all groups experienced hemolysis (Fig. 5d). SEM showed that MC3t3-E1 cells grew well under co-culture, and there was no significant difference in each group. These results indicate that MB/BG@LG and LG had good biocompatibility under light and no light conditions and could be used in future experiments and applications.

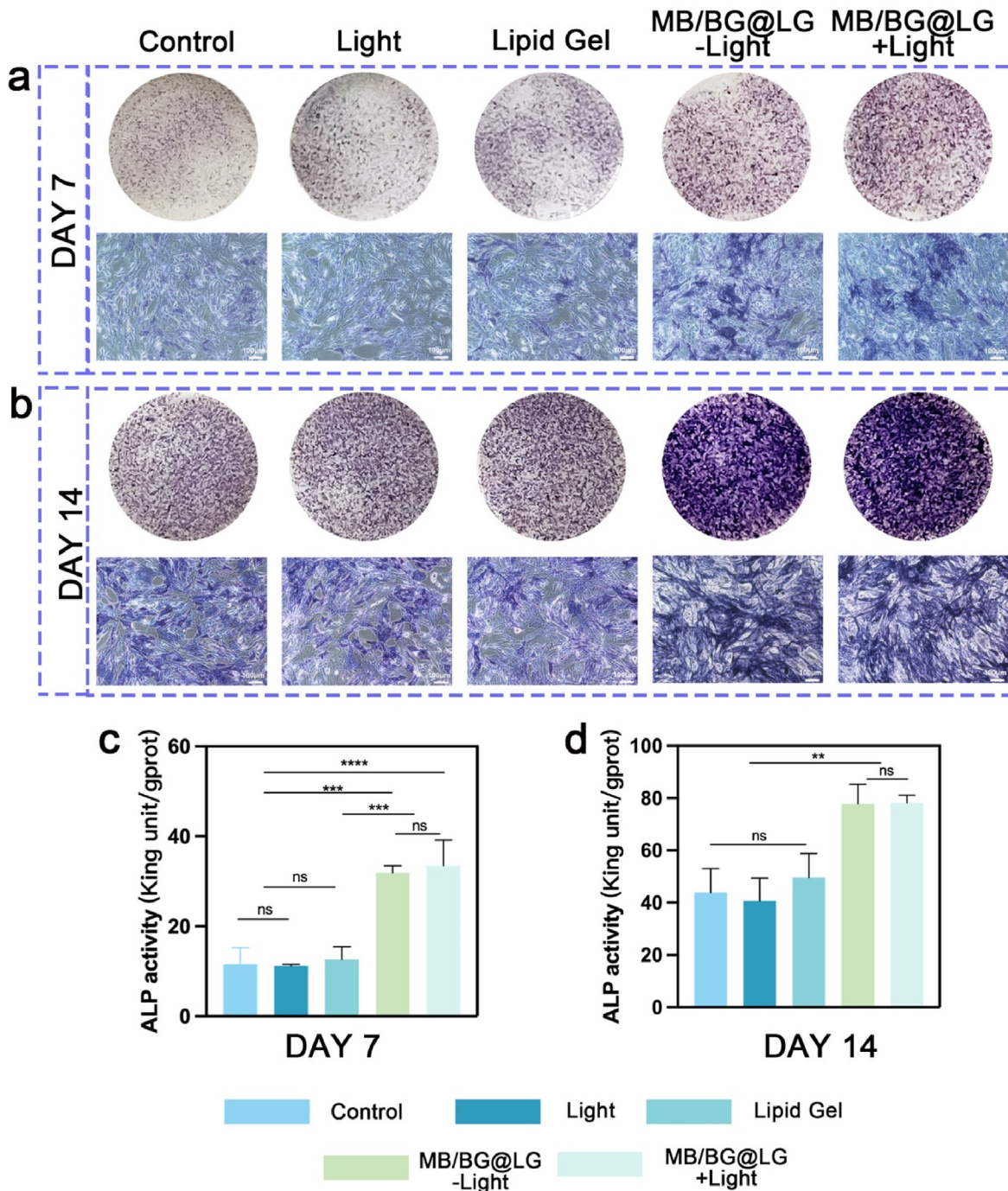


Fig. 6. The ALP staining photograph of MC3t3-E1 cultured with MB/BG@LG culture medium for day 7(a) and day 14(b). The quantitative analysis of alp on day 7 (c) and day14 (d).

3.5. Evaluation of osteogenic ability in vitro

Using ALP staining as an early indicator of osteogenic differentiation of ALP [48], we assessed the in vitro osteogenic differentiation ability of MB/BG/LG. As shown in Fig. 6a and b, on day 7 and 14, ALP staining in the MB/BG@LG + Light and MB/BG@LG-Light groups was significantly stronger than in the control, light, and light gel groups. On day 14, we observed that the staining of all components had deepened compared to that on day 7. The MB/BG@LG + Light and MB/BG@LG-Light groups were significantly stronger than the other components. Alp activity assay showed that MB/BG@LG (-Light) and MB/BG@LG (+Light) compared with control significantly promoted osteogenic differentiation ( $31.91 \pm 1.29$  and  $33.52 \pm 4.60$  vs  $11.62 \pm 3.67$  King unit/gprot) at day 7. The same trend was observed on day 14 and alp activity was enhanced compared with that on day 7 (Fig. 6c and 6d). Many studies have demonstrated that bioactive glass cells discharge a variety of ions into the body fluid milieu, modifying the local microenvironment to promote osteogenic differentiation [49–51]. As expected, MB/BG@LG containing

bioactive glass still promoted the ALP activity of MC3t3-E1 cells and had excellent osteogenic differentiation ability. MB/BG@LG, as a tissue engineering product, can be used to treat periodontitis-related alveolar bone abnormalities.

3.6. In vivo effect of bone regeneration and periodontal inflammatory response

The rat maxillary ligation-induced chronic periodontitis model [52] was used to assess the effectiveness of MB/BG@LG osteogenic antibacterial double-effect liposome gel for the treatment of periodontitis in vivo. First, 8-weeks female SD rats were anesthetized, and their maxillary second molar (M2) was ligated for 3 weeks. During modeling, regular local inoculations of *P. gingivalis* and 10% high-glucose feeding were performed (Fig. 7a). The level of alveolar bone loss was quantified by measuring the linear distance between the enamel cementum junction (CEJ) and apex of the alveolar bone crest (ABC). Micro-CT results showed that the CEJ-ABC distance was  $0.27 \pm 0.16$  mm in the healthy group and

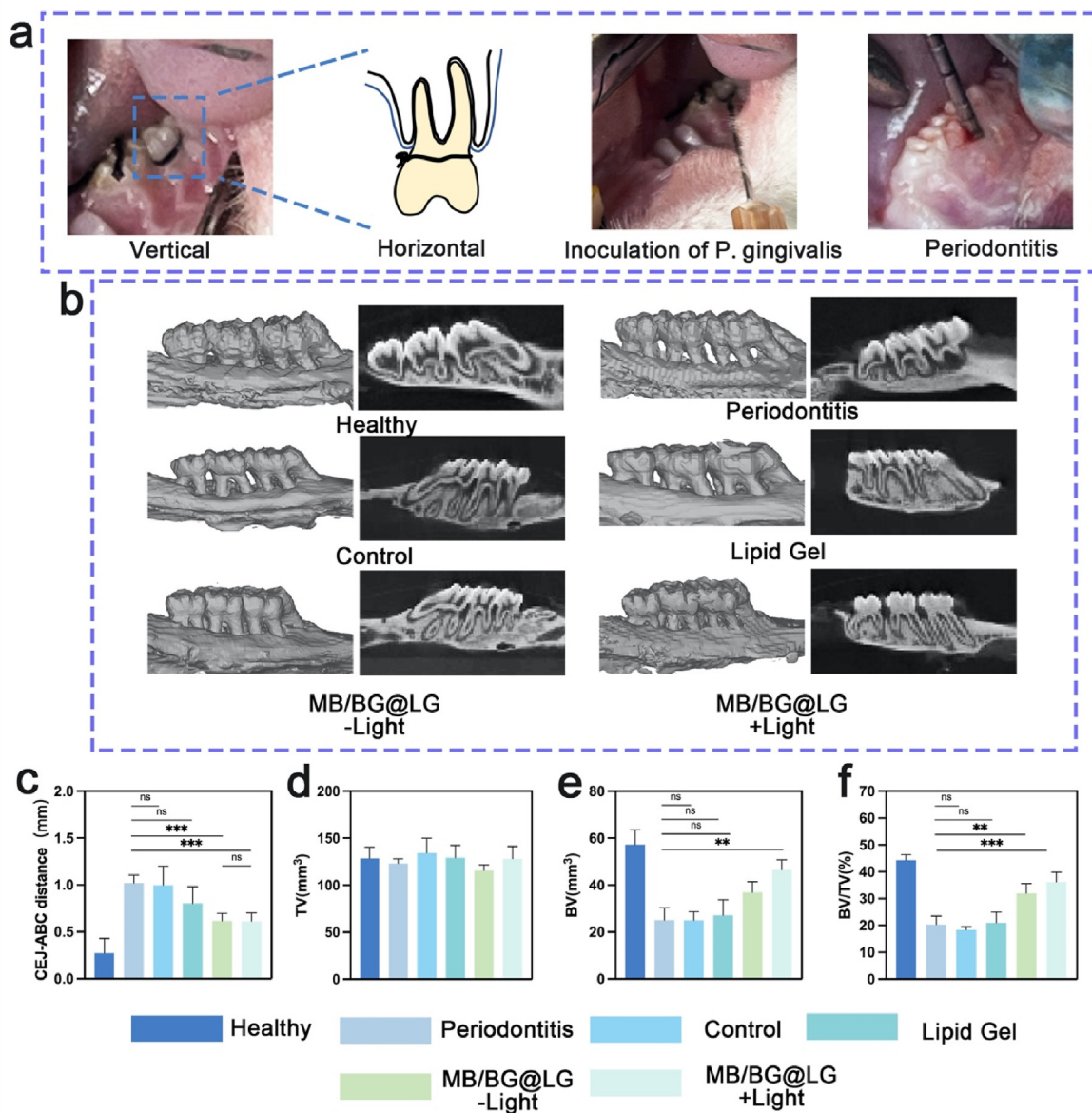
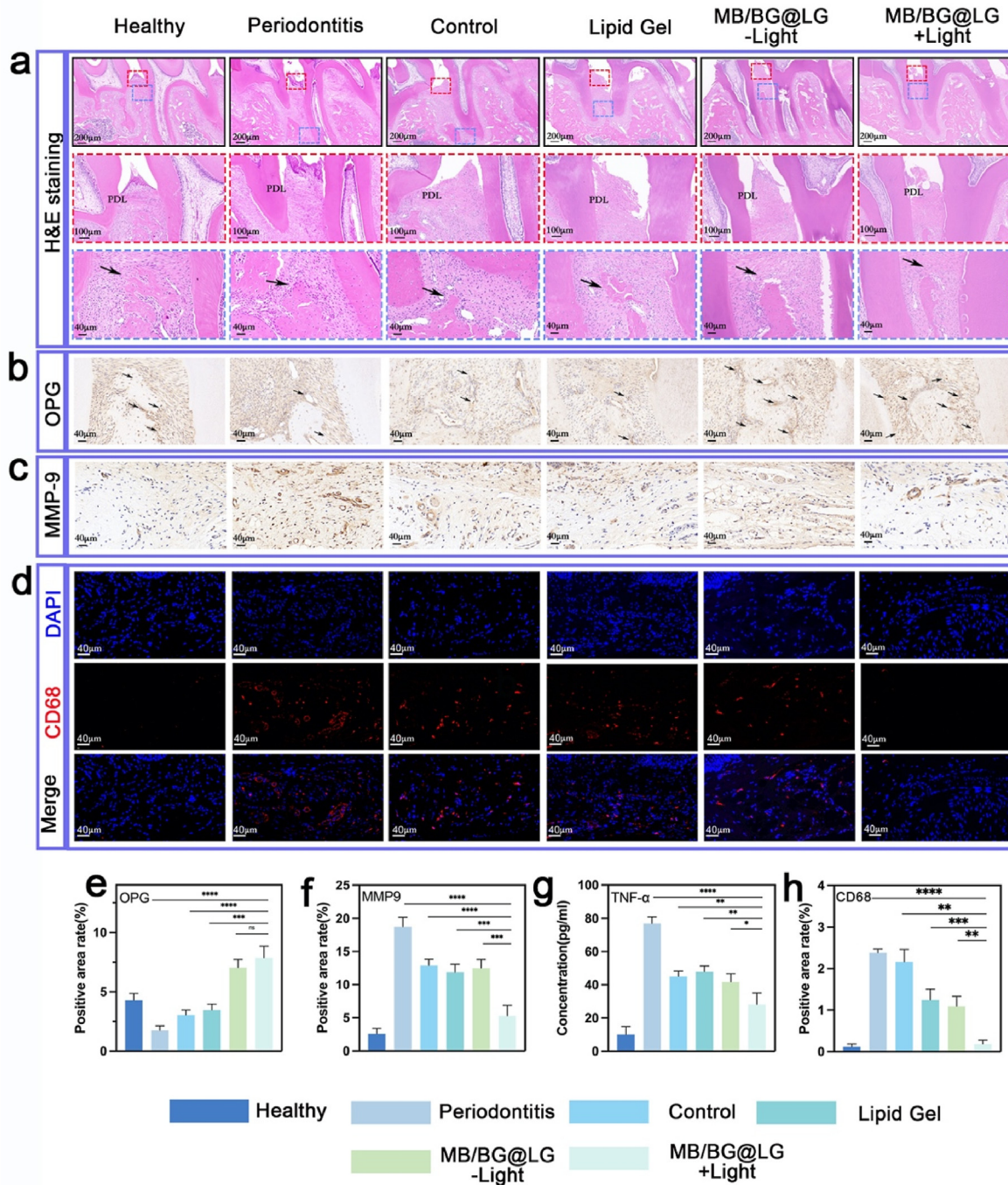


Fig. 7. (a) The modeling process in rats with periodontitis. (b) The three-dimensional micro-CT images of alveolar bone in the healthy rats, periodontitis rats and the rats treated with MB/BG@LG with and without 660 nm light. (c) CEJ-ABC distance on the buccal sides, (d) TV, (e) BV, (f) BV/TV calculate from micro-CT results. \*, \*\*and\*\*\*indicate  $p < 0.05$ ,  $p < 0.01$  and  $p < 0.001$ .

1.02 ± 0.09 mm in the periodontitis group, indicating that the periodontitis model had been successfully established (Fig. 7a,b,7c). Subsequently, periodontitis rat was relieved by the removal of ligation, and different treatments were administered. After 4 weeks, the CEJ-ABC distances in the control, the Lipid gel, the MB/BG@LG -light, and the MB/BG@LG + Light groups were 1.00 ± 0.21 mm, 0.80 ± 0.18 mm, 0.617 ± 0.08 mm, and 0.615 ± 0.09 mm, respectively. The MB/BG@LG + Light group outperformed the MB/BG@LG-Light group, but the difference was not statistically significant. These results indicate that both

MB/BG@LG-light group and MB/BG@LG + light group promoted alveolar bone regeneration in the presence of bioglass. The antibacterial effect produced by light to regulate the local inflammatory environment has a certain promoting effect on osteogenesis; however, this effect is a long-term and slow process that requires further observation.

Additionally, parameters associated with bones, such as BV, TV, and BV/TV, were measured. When there was no significant difference in TV between the groups, BV, and BV/TV in the MB/BG@LG-Light and MB/BG@LG + Light groups increased compared with those in the control and



**Fig. 8.** The H&E staining (a), OPG (b), MMP-9 (c) and CD68 (d) of healthy rats, periodontitis rats and the rats treated with blank, LG and MB/BG@LG with and without 660 nm light. The quantitative analysis of OPG (e) and MMP9 (f) expression of healthy rats, periodontitis rats and the rats treated with blank, LG and MB/BG@LG with and without 660 nm light. The TNF-α (g) and CD68 (h) expression of healthy rats, periodontitis rats and the rats treated with blank, LG and MB/BG@LG with and without 660 nm light.

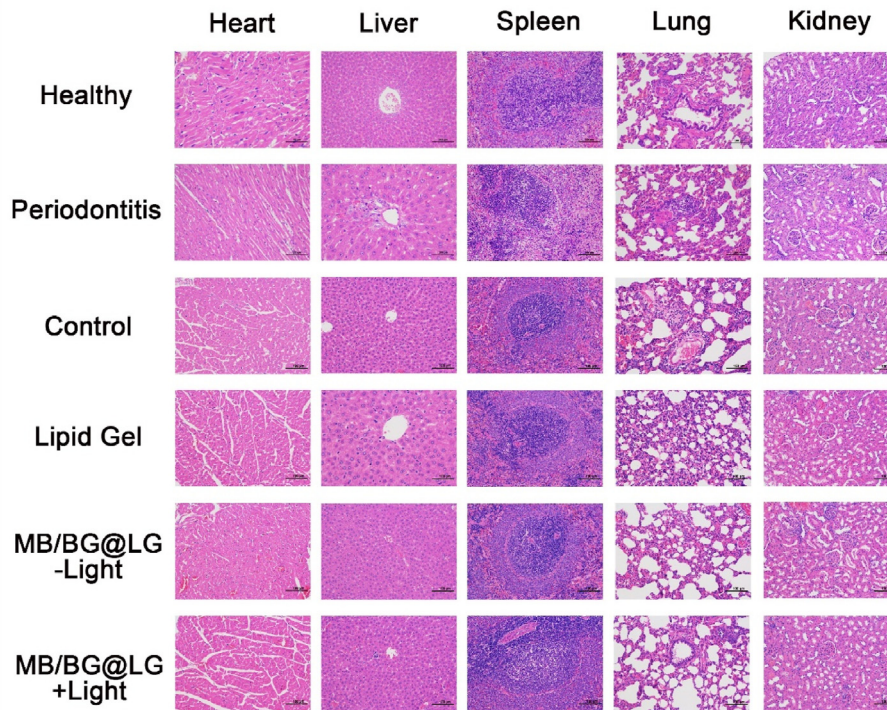


**Fig. 9.** The H&E staining of major organs (heart, liver, spleen, lung, and kidney) in healthy rats, periodontitis rats, and the rats treated with blank, LG, and MB/BG@LG with and without 660 nm light for 28 days.

lipid gel groups. These results further demonstrated that MB/BG@LG promoted alveolar bone regeneration owing to the presence of bioactive glass during osteogenesis (Figs. 7d, 8e and 9f).

H&E staining was used to further observe the regeneration of periodontal tissue and inflammatory infiltration between the maxillary first and second molars. The junctional epithelium was firmly attached to the enamel surface in the healthy group without any inflammatory cell infiltration. The alveolar crest located at the cemento-enamel junction indicated no obvious bone resorption. The periodontal ligament fibers were arranged in an orderly manner without rupture. In contrast, the periodontitis group exhibited many inflammatory cell infiltrations, breakage or disorder of periodontal fibers, and obvious proliferation of the binding epithelium to the root. In addition, the alveolar bone was significantly absorbed by the root, and the bone height was reduced. This indicated that the periodontitis model was successfully constructed, as shown in Fig. 8a. Compared to the other groups, MB/BG@LG + Light and MB/BG@LG-Light groups showed a significant increase in alveolar bone height due to the presence of bioglass. The progression of periodontitis was almost completely blocked in the MB/BG@LG + Light group, which was reflected by the close arrangement of epithelial cells and the lamina propria without obvious inflammatory cell aggregation.

To further quantify and evaluate the osteogenic effect, OPG was selected as an indicator of osteogenic differentiation and analyzed using immunohistochemical staining and ImageJ software. As shown in Fig. 8b and e, the OPG positive area rates of the MB/BG@LG + Light and MB/BG@LG-Light groups were  $7.85 \pm 1.00\%$  and  $7.041 \pm 0.67\%$ , respectively, which were statistically higher than Control group ( $3.04 \pm 0.41\%$ ) and Lipid gel group ( $3.45 \pm 0.50\%$ ). MB/BG@LG + Light had slightly higher OPG positive area rates than MB/BG@LG-light. Osteoprotegerin (OPG), a soluble decoy receptor released by osteoblasts, belongs to the TNF receptor (TNFr) superfamily. It inhibits the proliferation and operation of osteoclasts by preventing RANKL from binding to RANK [53, 54]. These results suggest that photodynamic antimicrobial therapy could inhibit the adhesion of biofilms by destroying pathogenic

microorganisms and the ionic interaction of bioactive glass to promote the regulation of bone homeostasis.

Finally, immunohistochemical staining of MMP9, immunofluorescence staining of macrophages (CD68), and an enzyme-linked immunosorbent assay (ELISA) were performed to further evaluate inflammation in gingival tissues. The positive expression of MMP-9 was highest in the periodontitis group ( $18.73 \pm 1.43\%$ ). After MB/BG@LG + light treatment ( $5.28 \pm 1.58\%$ ), MMP-9 levels were significantly decreased (Fig. 8c and f). MMP-9 is a gelatinase synthesized by neutrophils, as evidenced by numerous studies [55,56]. Degradation of gelatin and type IV collagen, as well as connective tissue loss, are strongly correlated with MMP9 over-expression. MMP9 expression also reflects the degree of inflammation and progression of periodontal disease [57]. The ROS produced by MB/BG@LG under illumination at 660 nm can effectively remove pathogenic microorganisms and reduce inflammatory responses. Jiang et al. proposed that methylene blue-mediated photodynamic therapy might not only slow the course of periodontitis by exerting an antimicrobial effect but also by causing over-infiltrating macrophages to induce apoptosis [58]. The expression of CD68 in the MB/BG@LG + Light group ( $0.18 \pm 0.09\%$ ) was considerably downregulated compared to Control group ( $2.16 \pm 0.30\%$ ), Lipid gel group ( $1.25 \pm 0.26\%$ ) and MB/BG@LG-Light group ( $1.09 \pm 0.24\%$ ), as revealed by immunofluorescence staining, which may be related to the regulation of macrophage apoptosis by ROS production (Fig. 8d and h). In addition, as shown in Fig. 8g, the content of TNF- $\alpha$  was  $45.07 \pm 3.15$  pg/mL for the Control group,  $47.82 \pm 3.44$  pg/mL for the Lipid gel group,  $41.75 \pm 4.95$  pg/mL for the MB/BG@LG-Light group and  $28.08 \pm 6.99$  pg/mL for the MB/BG@LG + Light group, TNF- $\alpha$  inflammation levels were significantly reduced in the MB/BG@LG + Light group after light exposure, and TNF- $\alpha$  also had a significant impact on regulating the severe local reactions associated with periodontitis [59]. TNF- $\alpha$  may trigger an inflammatory response, promote matrix metalloproteinase release, activate osteoclasts, and degrade the periodontal tissue. These inflammatory elements promote the incidence and progression of periodontitis by promoting the

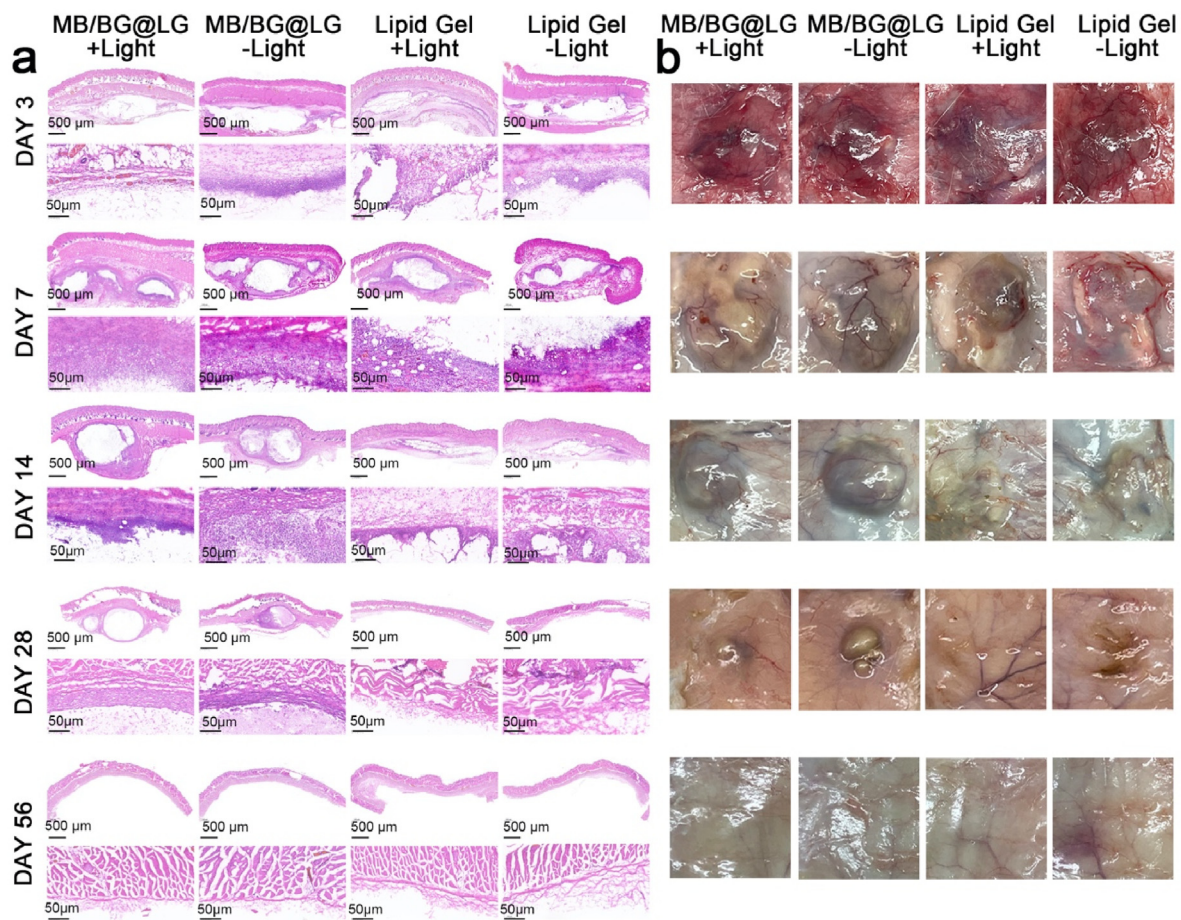


**Fig. 10.** (a) The H&E staining of the skin in the back after subcutaneous implantation of LG and MB/BG@LG for 3, 7, 14, 28, and 56 days. (b) The photograph of the skin in the back after subcutaneous implantation of LG and MB/BG@LG for 3, 7, 14, 28, and 56 days.

migration of pathogenic bacteria and their hazardous byproducts into deep tissues [60,61].

In conclusion, MB/BG@LG improved the periodontal inflammatory microenvironment and promoted the recovery of periodontal bone homeostasis by generating ROS to eliminate pathogenic microorganisms and reduce microbial attachment under light exposure, without obvious parenchymal organ damage (Fig. 9). Therefore, MB/BG@LG is a promising delivery system for periodontal therapy.

### 3.7. *In vivo* biosafety assessment

We further evaluated the *in vivo* toxicity and *in vivo* degradation capacity of hydrogels 200 μl lipid gel or MB/BG@LG injected subcutaneously into the backs of SD rats and treated with or without light. As shown in Fig. 10, the skin tissue in contact with the material was free of inflammation, suppuration, metaplasia, and necrosis. The lipid gel was completely degraded after 28 days without loading. MB/BG@LG containing bioglass was completely degraded after 56 days. These results indicate that MB/BG@LG has good biocompatibility and biosafety and can provide space and support for periodontal tissue osteogenesis at an early stage. This prevents epithelial connective tissue from entering the defect site prematurely and combining with the root surface to form a long-bound epithelium, which is not conducive to bone tissue regeneration and repair.

### Conclusion

In this study, a multi-functional and long-lasting drug delivery system was developed by encapsulating MB and bioglass into LG lipid precursor

by Macrosol technology. In addition, the system exhibited excellent adhesion properties, self-assembly properties, and superior drug release control capabilities, which improved the clinical feasibility of its application in complex oral environments. At the same time, the photodynamic therapy of MB and the sustainable release of BG ions resulted in the superior antibacterial properties and osteogenic effects of MB/BG@LG. MB/BG@LG demonstrated its bone regeneration and anti-inflammatory effects during the treatment of the rat periodontitis model. In conclusion, we believe that this innovative medication delivery technology has a significant potential for the therapeutic management of periodontal diseases.

### Statement of significance

There are many kinds of treatment methods for periodontitis, but it is still difficult to achieve the ideal purpose of alveolar bone repair and regeneration. In this study, an injectable lipid gel long-release system MB/BG@LG with osteogenic and antibacterial properties was developed for the treatment of periodontitis. 1) Injectable MB/BG@LG has excellent biocompatibility 2) ROS generated by MB/BG@LG can produce antibacterial effects to reduce inflammation while ions released by bioglass can promote osteogenic differentiation. 3) In the rat model of periodontitis, MB/BG@LG could be stably retained in the periodontal pocket by using the in-situ hydrosynthetic gel of the inflammatory exudate. MB/BG@LG can continuously inhibit bacteria, reduce inflammatory response, and promote periodontal tissue regeneration. In conclusion, we believe that MB/BG@LG can be used as a potential candidate for periodontal therapy.

## Credit author statement

Li Song and Fanrong Ai designed the study. Yeke Chen, Fang Dai and Tian Deng conducted experiments. Lijie Wang and Yuting Yang performed data analysis. Chenjiang He, Qiangdong Liu and Jianxin Wu collected the data. Li Song, Fanrong Ai and Yeke Chen wrote and revised the manuscript.

## Declaration of competing interest

The authors declare that they have no known competing financial interests or personal relationships that could have appeared to influence the work reported in this paper.

## Data availability

Data will be made available on request.

## Acknowledge

This work was supported by the National Natural Science Foundation of China (No. 82060203 to L.S. and No. 31960207 to F.A.) and the Interdisciplinary Innovation Fund of Natural Science, Nanchang University (No.9166-27060003-ZD04 to L.S.)

## Appendix A. Supplementary data

Supplementary data to this article can be found online at <https://doi.org/10.1016/j.mtbio.2023.100699>.

## References

- M. Nakajima, E.E.L. Tanner, N. Nakajima, K.N. Ibsen, S. Mitragotri, Topical treatment of periodontitis using an iongel, *Biomaterials* 276 (2021), 121069.
- N. Kassebaum, E. Bernabé, M. Dahiya, B. Bhandari, C. Murray, W. Marcenes, Global burden of severe periodontitis in 1990-2010: a systematic review and meta-regression, *J. Dent. Res.* 93 (11) (2014) 1045-1053.
- D.A.F. Nibali, L. G. Griffiths, K. Patel, J. Suvar, M.S. Tonetti, Severe periodontitis is associated with systemic inflammation and a dysmetabolic status: a case-control study, *J. Clin. Periodontol.* 34 (2007) 931-937.
- K.M.K. Xiaojing Li, LEIF TRONSTAD, INGAR OLSEN, Systemic diseases caused by oral infection, *Clin. Microbiol. Rev.* 13 (4) (2000) 547-558.
- S.M. Herrera D, S. Jepsen, I. Needleman, S. Roldán, A systematic review on the effect of systemic antimicrobials as an adjunct to scaling and root planing in periodontitis patients, *J. Clin. Periodontol.* 29 (2002) 136-159.
- G. Greenstein, Local drug delivery in the treatment of periodontal diseases: assessing the clinical significance of the results, *J. Periodontol.* 77 (4) (2006) 565-578.
- A. Brun, N. Moignot, M. Colombier, E. Dursun, Towards the nano-control of periodontal inflammation? *Oral Dis.* 26 (2) (2020) 245-248.
- N. Li, L. Jiang, H. Jin, Y. Wu, Y. Liu, W. Huang, L. Wei, Q. Zhou, F. Chen, Y. Gao, B. Zhu, X. Zhang, An enzyme-responsive membrane for antibiotic drug release and local periodontal treatment, *Colloids Surf. B Biointerfaces* 183 (2019), 110454.
- W. Xu, W. Tan, C. Li, K. Wu, X. Zeng, L. Xiao, Metformin-loaded  $\beta$ -TCP/CIS/SBA-15 composite scaffolds promote alveolar bone regeneration in a rat model of periodontitis, *J. Mater. Sci. Mater. Med.* 32 (12) (2021) 145.
- X. Xu, Y. Zhou, K. Zheng, X. Li, L. Li, Y. Xu, 3D polycaprolactone/gelatin-oriented electrospun scaffolds promote periodontal regeneration, *ACS Appl. Mater. Interfaces* 14 (41) (2022) 46145-46160.
- N. Chen, R. Ren, X. Wei, R. Mukundan, G. Li, X. Xu, G. Zhao, Z. Zhao, S.M. Lele, R.A. Reinhardt, D. Wang, Thermoresponsive hydrogel-based local delivery of simvastatin for the treatment of periodontitis, *Mol. Pharm.* 18 (5) (2021) 1992-2003.
- H. Guo, S. Huang, X. Yang, J. Wu, T.B. Kirk, J. Xu, A. Xu, W. Xue, Injectable and self-healing hydrogels with double-dynamic bond tunable mechanical, gel-sol transition and drug delivery properties for promoting periodontium regeneration in periodontitis, *ACS Appl. Mater. Interfaces* 13 (51) (2021) 61638-61652.
- B. Bai, C. Gu, X. Lu, X. Ge, J. Yang, C. Wang, Y. Gu, A. Deng, Y. Guo, X. Feng, Z. Gu, Polydopamine functionalized mesoporous silica as ROS-sensitive drug delivery vehicles for periodontitis treatment by modulating macrophage polarization, *Nano Res.* 14 (12) (2021) 4577-4583.
- X. Bao, J. Zhao, J. Sun, M. Hu, X. Yang, Polydopamine nanoparticles as efficient scavengers for reactive oxygen species in periodontal disease, *ACS Nano* 12 (9) (2018) 8882-8892.
- S. Subramaniam, Y.H. Fang, S. Sivasubramanian, F.H. Lin, C.P. Lin, Hydroxyapatite-calcium sulfate-hyaluronic acid composite encapsulated with collagenase as bone substitute for alveolar bone regeneration, *Biomaterials* 74 (2016) 99-108.
- Y. Liu, T. Li, M. Sun, Z. Cheng, W. Jia, K. Jiao, S. Wang, K. Jiang, Y. Yang, Z. Dai, L. Liu, G. Liu, Y. Luo, ZIF-8 modified multifunctional injectable photopolymerizable GelMA hydrogel for the treatment of periodontitis, *Acta Biomater.* 146 (2022) 37-48.
- Y.L. Donglin Han, Xiangmei Liu, Kelvin Wai, Kwok Yeung, Yufeng Zheng, Zhenduo Cui, Yanqin Liang, Zhaoyang Li, Shengli Zhu, Xianbao Wang, Shuillin Wu, Phototherapy-strengthened photocatalytic activity of polydopamine-modified metal-organic frameworks for rapid therapy of bacteria-infected wounds, *J. Mater. Sci. Technol.* 62 (2021) 83-85.
- J. Li, Z. Li, X. Liu, C. Li, Y. Zheng, K. Yeung, Z. Cui, Y. Liang, S. Zhu, W. Hu, Y. Qi, T. Zhang, X. Wang, S. Wu, Interfacial engineering of BiS/TiCT MXene based on work function for rapid photo-excited bacteria-killing, *Nat. Commun.* 12 (1) (2021) 1224.
- C. Ghosh, P. Sarkar, R. Issa, J. Haldar, Alternatives to conventional antibiotics in the era of antimicrobial resistance, *Trends Microbiol.* 27 (4) (2019) 323-338.
- M. Wainwright, T. Maisch, S. Nonell, K. Plaetzer, A. Almeida, G.P. Tegos, M.R. Hamblin, Photoantimicrobials-are we afraid of the light? *Lancet Infect. Dis.* 17 (2) (2017) e49-e55.
- J. Zhang, Q. Jia, Z. Yue, J. Huo, J. Chai, L. Yu, R. Nie, H. Shao, Y. Zhao, P. Li, W. Huang, An electroluminescent flexible device for highly efficient eradication of drug-resistant bacteria, *Adv. Mater.* 34 (17) (2022), e2200334.
- A. Späth, C. Leibl, F. Cieplik, K. Lehner, J. Regensburger, K.A. Hiller, W. Bäuml, G. Schmalz, T. Maisch, Improving photodynamic inactivation of bacteria in dentistry: highly effective and fast killing of oral key pathogens with novel tooth-colored type-II photosensitizers, *J. Med. Chem.* 57 (12) (2014) 5157-5168.
- S. Liu, Y.N. Wang, B. Ma, J. Shao, H. Liu, S. Ge, Gingipain-responsive thermosensitive hydrogel loaded with SDF-1 facilitates in situ periodontal tissue regeneration, *ACS Appl. Mater. Interfaces* 13 (31) (2021) 36880-36893.
- X. Xu, Z. Gu, X. Chen, C. Shi, C. Liu, M. Liu, L. Wang, M. Sun, K. Zhang, Q. Liu, Y. Shen, C. Lin, B. Yang, H. Sun, An injectable and thermosensitive hydrogel: promoting periodontal regeneration by controlled-release of aspirin and erythropoietin, *Acta Biomater.* 86 (2019) 235-246.
- S. Zhao, H. Wang, Y. Zhang, W. Huang, M.N. Rahaman, Z. Liu, D. Wang, C. Zhang, Copper-doped borosilicate bioactive glass scaffolds with improved angiogenic and osteogenic capacity for repairing osseous defects, *Acta Biomater.* 14 (2015) 185-196.
- E. Zeimaran, S. Pourshahrestani, I. Djordjevic, B. Pinguan-Murphy, N.A. Kadri, M.R. Towler, Bioactive glass reinforced elastomer composites for skeletal regeneration: a review, *Mater Sci Eng C Mater Biol Appl* 53 (2015) 175-188.
- X. Wang, L. Huang, Y. Zhang, F. Meng, M. Donoso, R. Haskell, L. Luo, Tunable two-compartment on-demand sustained drug release based on lipid gels, *J. Pharmaceut. Sci.* 109 (2) (2020) 1059-1067.
- L. Huang, Y. Li, Y. Du, Y. Zhang, X. Wang, Y. Ding, X. Yang, F. Meng, J. Tu, L. Luo, C. Sun, Mild photothermal therapy potentiates anti-PD-L1 treatment for immunologically cold tumors via an all-in-one and all-in-control strategy, *Nat. Commun.* 10 (1) (2019) 4871.
- J.B. Maria Wadsäter, Tommy Nylander, Fredrik Tiber, Formation of highly structured cubic micellar lipid nanoparticles of soy phosphatidylcholine and glycerol dioleate and Their Degradation by triacylglycerol lipase, *ACS Appl. Mater. Interfaces* 6 (2014) 7063-7069.
- J.C. Barauskas, C. M. Jankunec, M. Spandyreva, K. Ribokaite, F. Tiber, M. Johnsson, Interactions of lipid-based liquid crystalline nanoparticles with model and cell membranes, *Int. J. Pharm.* 391 (2010) 284-291.
- A. Linkeviūtė, J. Būdienė, E. Naujalis, A. Katalnikovas, J. Barauskas, accepted article characterisation and stability study of cranberry flavonoids in lipid liquid crystalline systems.
- J.W. Chenyu Guo, Fengliang Cao, Robert J. Lee, Guangxi Zhai, Lyotropic liquid crystal systems in drug delivery, *Drug Discov. Today* 15 (2010) 23-24.
- T.S. Rosenbaum E, L.B. Johansson, A characterisation study on the application of inverted lyotropic phases for subcutaneous drug release, *Int. J. Pharm.* 388 (2010) 52-57.
- F. Tiber, J. Roberts, C. Cervin, M. Johnsson, S. Sarp, A. Tripathi, M. Linden, Octreotide s.c. depot provides sustained octreotide bioavailability and similar IGF-1 suppression to octreotide LAR in healthy volunteers, *Br. J. Clin. Pharmacol.* 80 (3) (2015) 460-472.
- P. Jia, C. Bo, L. Hu, Y. Zhou, Synthesis and characterization of glyceryl monooleate-based polyester, *Kor. J. Chem. Eng.* 32 (2015) 547-551.
- K. Zhang, X. Zhang, H. Sun, X. Li, J. Bai, Q. Du, C. Li, Modulated photoluminescence and photodynamic efficiency of hydroxyapatite-methylene blue@carbon-ions by ion- $\pi$  coupling interactions, *Colloids Surf. A Physicochem. Eng. Asp.* 634 (2022), 127927.
- J. Hum, A.R. Boccaccini, Collagen as coating material for 45S5 bioactive glass-based scaffolds for bone tissue engineering, *Int. J. Mol. Sci.* 19 (6) (2018).
- A. Angelova, B. Angelov, R. Mutafchieva, S. Lesieur, P. Couvreur, Self-assembled multicompartiment liquid crystalline lipid carriers for protein, peptide, and nucleic acid drug delivery, *Acc. Chem. Res.* 44 (2) (2011) 147-156.
- X.L. Xian-Fu Zhang, The photostability and fluorescence properties of diphenylisobenzofuran, *J. Lumin.* 131 (2011) 2263-2266.
- S. Pemi, C. Piccirillo, J. Pratten, P. Prokopovich, W. Chrzanowski, I. Parkin, M. Wilson, The antimicrobial properties of light-activated polymers containing methylene blue and gold nanoparticles, *Biomaterials* 30 (1) (2009) 89-93.

- [41] Z. Wang, G. Zhang, Y. Li, Preparation of chitosan/polyacrylamide/graphene oxide composite membranes and study of their methylene blue adsorption properties, *Materials* 13 (19) (2020).
- [42] X. Tong, X. Qi, R. Mao, W. Pan, M. Zhang, X. Wu, G. Chen, J. Shen, H. Deng, R. Hu, Construction of functional curdlan hydrogels with bio-inspired polydopamine for synergistic periodontal antibacterial therapeutics, *Carbohydr. Polym.* 245 (2020), 116585.
- [43] J. Schwiertz, A. Wiehe, S. Gräfe, B. Gitter, M. Eppe, Calcium phosphate nanoparticles as efficient carriers for photodynamic therapy against cells and bacteria, *Biomaterials* 30 (19) (2009) 3324–3331.
- [44] F.F. Gabriela Alves da Collina, Thabata Paulino da Costa Santos, Natalia Gesse Sobrinho, Simone Aquino, Renato Araújo Prates, Daniela de Fátima Teixeira da Silva, Anna Carolina Ratto Tempestini Horliana, Christiane Pavani, Controlling methylene blue aggregation: a more efficient alternative to treat *Candida albicans* infections using photodynamic therapy, *Photochem. Photobiol. Sci.* 17 (2018) 1355–1364.
- [45] Y.Z. Yi Zhuo, Bing Wang, Shiqi Cheng, Raorao Yuan, Shaowen Liu, Mailin Zhao, Bin Xu, Yan Zhang, Xiaolei Wang, Gold Nanocluster & Indocyanine Green Based Triple-Effective Therapy for MRSA Infected Central Nervous System, *Applied Materials Today*, 2022.
- [46] X. Zhao, Y. Yang, J. Yu, R. Ding, D. Pei, Y. Zhang, G. He, Y. Cheng, A. Li, Injectable hydrogels with high drug loading through B-N coordination and ROS-triggered drug release for efficient treatment of chronic periodontitis in diabetic rats, *Biomaterials* 282 (2022), 121387.
- [47] S. Fan, X. Wu, Z. Fang, G. Yang, J. Yang, W. Zhong, J. Luo, M. Xing, W. Wan, Injectable and ultra-compressible shape-memory mushroom: highly aligned microtubules for ultra-fast blood absorption and hemostasis, *Chem. Eng. J.* 460 (2023), 140554.
- [48] Y. Zhu, H. Liang, X. Liu, J. Wu, C. Yang, T. Wong, K. Kwan, K. Cheung, S. Wu, K. Yeung, Regulation of macrophage polarization through surface topography design to facilitate implant-to-bone osteointegration, *Sci. Adv.* 7 (14) (2021).
- [49] M. Ojansivu, S. Vanhatupa, L. Björkvik, H. Häkkinen, M. Kellomäki, R. Autio, J. Ihalainen, L. Hupa, S. Miettinen, Bioactive glass ions as strong enhancers of osteogenic differentiation in human adipose stem cells, *Acta Biomater.* 21 (2015) 190–203.
- [50] A. Hoppe, N. Güldal, A. Boccaccini, A review of the biological response to ionic dissolution products from bioactive glasses and glass-ceramics, *Biomaterials* 32 (11) (2011) 2757–2774.
- [51] J.R. Jones, Review of bioactive glass: from Hench to hybrids, *Acta Biomater.* 9 (2013) 4457–4486.
- [52] C.G. Bingbing Bai, Xiaohui Lu, Xingyu Ge, Junling Yang, Chenfei Wang, Yongchun Gu, Aidong Deng, Yuehua Guo, Xingmei Feng, Zhifeng Gu, Polydopamine functionalized mesoporous silica as ROS-sensitive drug delivery vehicles for periodontitis treatment by modulating macrophage polarization, *Nano Res.* (2021) 1–7.
- [53] O.F. Yehuda Klein, Stabholz Ayala, Stella Chaushu, David Polak, Bone regeneration with bovine bone impairs orthodontic tooth movement despite proper osseous wound healing in a novel mouse model, *J. Periodontol.* 90 (2019) 189–199.
- [54] T.O.S. Raimundo, Fernandes de Araújo Júnior 1, caroline addison Xavier de Medeiros, Lélia batista de Souza, maria de Lourdes Freitas, Hévio freitas de Lucena, maria do socorro costa feitosa alves, aurigena antunes de Araújo, Carvedilol decrease IL-1 $\beta$  and TNF- $\alpha$ , Inhibits MMP-2, MMP-9, COX-2, and RANKL Expression, and Up-Regulates OPG in a Rat Model of Periodontitis, *PLoS One* 8 (7) (2013), e66391.
- [55] A.P.G. Isola, V. Ronsivalle, A. Alibrandi, G. Palazzo, A. Lo Giudice, Impact of matrix metalloproteinase-9 during periodontitis and cardiovascular diseases, *Molecules* 26 (2021) 1777.
- [56] H.R.P.C. Franco, S. Timo, B. Claudia, H. Marcela, Matrix metalloproteinases as regulators of periodontal inflammation, *Int. J. Mol. Sci.* 18 (2) (2017).
- [57] Y.Y. Xiaodan Zhao, Yu Jing, Rui Ding, Dandan Pei, Yanfeng Zhang, Gang He, Yilong Cheng, Ang Li, Injectable hydrogels with high drug loading through B–N coordination and ROS-triggered drug release for efficient treatment of chronic periodontitis in diabetic rats, *Biomaterials* 282 (2022), 121387.
- [58] W.Y. Chunlan Jiang, Chengyi Wang, Wei Qin, Jiajun Ming, Manman Zhang, Haixin Qian, Ting Jiao, Methylene Blue-Mediated Photodynamic Therapy Induces Macrophage Apoptosis via ROS and Reduces Bone Resorption in Periodontitis, *Oxid Med Cell Longev.* 2019.
- [59] H.D. Algate K, P.M. Bartold, T.N. Crotti, M.D. Cantley, The Effects of Tumour Necrosis Factor- $\alpha$  on Bone Cells Involved in Periodontal Alveolar Bone Loss; Osteoclasts, Osteoblasts and Osteocytes, *J Periodontal Res.* 2016.
- [60] B. Z, TNF and bone remodeling, *Curr. Osteoporos. Rep.* 15 (3) (2017) 126–134.
- [61] B.T. Yucel-Lindberg, T Båge, Inflammatory mediators in the pathogenesis of periodontitis, *Expet Rev. Mol. Med.* 15 (2013) article e7.